

# Gaussian-Based and Outside-the-Box Runtime Monitoring Join Forces <sup>★</sup>

Vahid Hashemi<sup>1</sup>, Jan Křetínský<sup>2,3</sup> , Sabine Rieder<sup>3,1,2</sup> , Torsten Schön<sup>4</sup>,  
and Jan Vorhoff<sup>1,4</sup>

<sup>1</sup> Audi AG, Ingolstadt, Germany

<sup>2</sup> Masaryk University, Brno, Czech

<sup>3</sup> Technical University of Munich, Munich, Germany

<sup>4</sup> Almotion Bavaria, Technische Hochschule Ingolstadt, Ingolstadt, Germany

**Abstract.** Since neural networks can make wrong predictions even with high confidence, monitoring their behavior at runtime is important, especially in safety-critical domains like autonomous driving. In this paper, we combine ideas from previous monitoring approaches based on observing the activation values of hidden neurons. In particular, we combine the Gaussian-based approach, which observes whether the current value of each monitored neuron is similar to typical values observed during training, and the Outside-the-Box monitor, which creates clusters of the acceptable activation values, and, thus, considers the correlations of the neurons' values. Our experiments evaluate the achieved improvement.

## 1 Introduction

*Neural Networks (NNs)* show impressive results on a variety of computer vision tasks [2, 13, 21, 24]. However, studies demonstrate that even state-of-the-art NNs experience reduced accuracy when processing so-called *Out-Of-Distribution (OOD) data*, which follows a different distribution than the *In-Distribution (ID) data* used during training [16, 18, 19]. Furthermore, even very well-trained NNs fail to reach perfect accuracy on the testing data, although it is ID. Such unavoidable inaccuracy poses a significant challenge in safety-critical domains like autonomous driving and highlights the need for runtime monitors that hint at uncertain, and, thus, possibly erroneous, predictions.

*Out-Of-Model-Scope (OMS) detection* [6] is the task of identifying inputs leading to incorrect predictions. Monitors targeting the OMS setting aim to

---

<sup>★</sup> The authors would like to thank all partners within the Hi-Drive project for their cooperation and valuable contribution. This project has received funding from the European Union's Horizon 2020 research and innovation program under grant agreement No 101006664 and the MUNI Award in Science and Humanities (MUNI/I/1757/2021) of the Grant Agency of Masaryk University. The sole responsibility of this publication lies with the authors. Neither the European Commission nor CINEA – in its capacity of Granting Authority – can be made responsible for any use that may be made of the information this document contains.

identify OOD and ID data for which the NN produces incorrect results, but, in contrast to OOD detection, should not notify of correctly processed OOD data. Since the primary objective of runtime monitoring is identifying erroneous outcomes, OMS detection is more adequate in a safety-critical context than OOD detection. Nevertheless, OOD detection may serve as a valuable proxy to attain the ultimate goal of OMS detection.

In this work, we combine ideas of two existing lightweight OOD detection approaches, namely the Gaussian monitor [7] and the Outside-the-Box monitor [8] (short: Box monitor) and evaluate the combination for OMS detection. Both approaches base their OOD decision on the activation values of an inner, typically the penultimate, layer. The Box monitor records the activation values of known data and creates areas of previously seen activation value vectors in the form of unions of hyperrectangles. Inputs producing values inside the box are assumed to be safe. The Gaussian monitor [7] instead models the activation values of a neuron as a Gaussian distribution and computes intervals that contain *likely* values of this distribution. Consequently, it ignores outliers in training and warns against rare values. However, the Gaussian monitor does not use the information of correlations between neurons used in the Box monitor as it, technically, only considers one hyperrectangle. Our combination of the two approaches enriches the Gaussian monitor with information about these correlations among the individual neurons. As the amount of computations increases with the number of monitored neurons, we decrease the number of monitored neurons by using partial gradient descent.

Our basic experiments in the OMS setting show that considering the correlations of neurons improves the detection capabilities of the vanilla Gaussian monitor for the complex CIFAR-10 [11] dataset. In contrast, on the simpler GTSRB [9] dataset, the combination of the Box monitor and the Gaussian monitor achieves similar results as the latter. Interestingly, reducing the number of monitored neurons does not drastically decrease performance for the combined monitor, which altogether allows for more efficient runtime monitoring.

*Our contribution* can be summarized as follows:

- We extend the monitor presented in [7] to benefit from clustering of activation values from the Box monitor [8].
- As the computation requirements increase with the size of the NN, we investigate monitoring only the most relevant neurons of the NN.
- We evaluate the presented monitoring approaches for OMS detection on the CIFAR-10 and GTSRB datasets.

## 2 Related Work

As our work focuses on detecting OMS data based on the activation values of hidden layers in the NN, we mention related work following the same approach. The survey by Yang et al. [23] presents a more comprehensive overview of OOD detection approaches.

Cheng et al. [3] focus on the status (equal to zero or above zero) of ReLU neurons on known safe data and store it as a “pattern”. Patterns observed at runtime are accepted if they are close to already stored patterns. Henzinger et al. [8] consider the activation values and build safe areas in the form of hyper-rectangles based on the observed values. Lukina et al. [14] extend the approach to incrementally adapt at runtime and create a quantitative measure of how unknown a new sample is. Hashemi et al. [7] model the activation values of a neuron with a Gaussian distribution and build an interval containing common activation values centered around the mean of the distribution. Sun et al. [20] use the distance of an activation value to its k-nearest neighbor in a set of previously recorded activation values as OOD score. Morteza and Li [15] assume that the activation values of ID data follow a multivariate Gaussian distribution and measure the sum of values proportional to each class log-likelihood of the in-distribution data. Lee et al. [12] fit a class-dependent multivariate Gaussian distribution to the observed activation values of a softmax classifier and compute a score based on the Mahalanobis-distance. Corbière et al. [5] suggest using an NN trained on the neuron activation values of the penultimate layer as a monitor. This NN is supposed to predict the probability of the monitored NN making a correct prediction for the input.

### 3 Preliminaries

#### 3.1 Neural Networks

An NN consists of  $m$  layers  $L_1$  to  $L_m$  and each layer  $l$  contains  $s_l$  neurons. Each neuron of layer  $l > 1$  first computes its pre-activation value  $\mathbf{z}$  as weighted sum of activation values from neurons of the previous layer. The neuron’s activation value  $\mathbf{a}$  is obtained by applying an activation function  $f_l : \mathbb{R} \rightarrow \mathbb{R}$  to the pre-activation value. With a slight abuse of notation, we write  $f_l(\mathbf{z})$  when we refer to component-wise application of  $f_l$  on  $\mathbf{z}$ . We formalize the computations for a layer  $l$  with weight matrix  $W_l \in \mathbb{R}^{s_{l-1} \times s_l}$ , bias  $\mathbf{b}_l$  and input  $\mathbf{x} \in D \subseteq \mathbb{R}^n$  as:

$$\mathbf{a}_0 = \mathbf{x} \quad \mathbf{z}_l = W_l^T \mathbf{a}_{l-1} + \mathbf{b}_l \quad \mathbf{a}_l = f_l(\mathbf{z}_l)$$

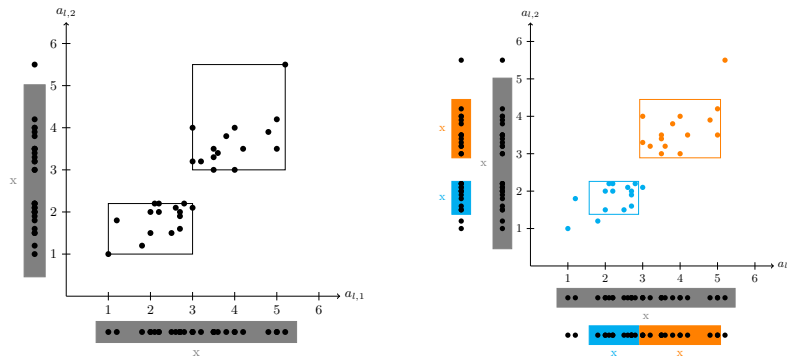
The last layer provides the classification result, meaning the mapping of data-point  $\mathbf{x}$  to a set of  $r$  different labels  $Y = \{y_1, \dots, y_r\}$ .

#### 3.2 Monitors

**Gaussian Monitor [7].** The approach consists of three steps: Training of the monitor, threshold setting and runtime evaluation. In the training process, for each neuron and class, a Gaussian distribution is fitted to the neuron’s activation values observed for several ID inputs. We then compute an interval for each neuron containing approximately 95% of recorded activation values based on the empirical rule [22]. Due to the use of the empirical rule, it is barely ever the case that all neurons produce values contained in their respective intervals. This

is rectified by setting a threshold on the number of neurons that need to produce such values. A higher threshold will lead to the monitor classifying more images as OOD and vice versa. We consider a set of known safe images not used for training the monitor for setting this threshold. Lastly, when the NN receives a new sample as input, the neurons' activation values and the predicted class are observed. Each neuron votes if its value lies inside the bounds for the predicted class, and the outcome of the vote is compared to the threshold.

**Box Monitor [8].** Henzinger et al. suggest using multidimensional boxes for monitoring, one set of boxes for each class. The boxes are computed based on activation values observed on ID inputs. These values are clustered with the K-Means algorithm and each cluster results in one box. As there exists a trade-off between the number of correctly identified OOD points and wrongly identified ID data, it is possible to modify the coarseness of the boxes by enlarging them by a factor of  $\gamma$ . During runtime, the authors expect ID data to produce activation vectors contained in the boxes and OOD data to produce values outside of it.



(a) Comparison of the Gaussian monitor and the Box monitor. The figure is based on [7].

(b) Comparison of Gaussian monitor and the clustered Gaussian monitor. The colors denote the assigned point cluster.

Fig. 1: Comparison of different monitors. The axes represent the neurons and their activation values, and the points are the vectors of activation values observed for a particular input. Boxes depict safe areas of the Box and the combined monitor. The points below each axis show the activation values mapped to the specific axis with  $x$  highlighting the mean. The boxes below the axes depict the activation values the Gaussian monitor accepts.

**Difference between Gaussian and Box Monitor.** Figure 1a depicts the differences between the two described monitors. While the Box Monitor considers the relationship between neurons, the Gaussian monitor models the behavior of each single neuron more precisely and is less affected by outliers.

### 3.3 Neuron Selection via Gradient Analysis

Due to the additional complexity each new neuron brings to monitoring, Cheng et al. [3] propose, among other things, only observing the most relevant neurons in the monitored layer  $L_l$ . They identify these neurons through the absolute value of the partial gradient  $|\frac{\partial a_{m,j}}{\partial a_{l,t}}|$  for activation value  $a_{m,j}$  of neuron  $N_{m,j}$  in the output layer  $L_m$ , and the activation  $a_{l,t}$  of a neuron  $N_{l,t} \in L_l$ . The partial derivatives depend on the activation function’s derivatives and vary for each input. A special case is monitoring last hidden layer without any non-linear computation. In this particular case, as pointed out by Cheng et al. [3], the partial derivatives are the weights between the two layers. The paper is unclear on handling the case with different partial derivatives for various inputs.

## 4 Methodology

### 4.1 Combining Gaussian Monitor and Box Monitor

We combine the Box monitor and the Gaussian monitor to obtain a monitor robust to outliers (like the Gaussian monitor) and aware of neuron correlations (like the Box monitor). The monitor is trained based on an observation of  $k$  activation vectors for each class  $c$ . These  $k$  activation vectors are obtained from correctly classified ID data and are clustered using K-Means similar to the creation of the Box monitor. Overall, we obtain several clusters per class. The Gaussian Monitor is called on each cluster separately and computes a Gaussian distribution for each neuron and its activation values belonging to the clusters. Based on the distribution, intervals containing 95% of the data are computed as before and boxes are build based on these intervals. Fig. 1b shows the boxes for different clusters (depicted by different colors). For an input to be accepted, its activation value needs to be contained in one of the boxes. While the Gaussian monitor from Fig. 1a would have accepted an activation value of  $(2, 4)$ , the new monitor will mark it correctly as previously unseen. Furthermore, the combined monitor is more sensitive to cluster outliers than the Box monitor. The sensitivity can be fine tuned by setting a threshold on how many neurons need to produce values contained inside the intervals of a specific cluster. Due to the new structure of the monitor, we use a procedure similar to Henzinger et al. [8] for detecting outliers at runtime. When a new input is observed, we compute the Euclidean distance of its activation value vector to the centroids of each cluster and compare to the closest ones. For each cluster, each neuron still votes on whether its activation is in the interval and thus valid and an alarm will be triggered if the number is lower than the threshold.

One can also use a multivariate Gaussian distribution for each cluster and compute the Mahalanobis distance similar to the suggestion by Lee et al. [12].

### 4.2 Neuron Selection for Monitoring

To improve the runtime performance of our proposed monitors, we adhere to the suggestion made by Cheng et al. [3] to only observe the neurons with the most

significant impact on the expected class score determined by partial gradient analysis. We compute a score  $abs\_score_{j,t}^l$  for a particular class  $y_j$  and a neuron  $N_{l,t}$  of layer  $l$  based on the partial derivative of several known safe inputs. We define  $S_j \subset D$  as a set of known safe inputs of class  $j$ . To calculate the  $abs\_score_{j,t}^l$  for the  $N_{l,t}$ , we sum up the absolute value of the partial gradient  $\frac{\partial a_{m,j}(x_i)}{\partial a_{l,t}(x_i)}$  for each input vector  $\mathbf{x}_i \in S_j$ , where  $a_{m,j}(x_i)$  represents the activation value of neuron  $N_{m,j}$  when the NN is applied to  $x_i$ :

$$abs\_score_{j,t}^l = \sum_{i=1}^{|S_j|} \left| \frac{\partial a_{m,j}(x_i)}{\partial a_{l,t}(x_i)} \right|.$$

While we can apply this technique of selection relevant neurons to the NN we want to monitor, there is also the possibility to use a *monitoring NN* [5]. In this case, we first train an NN on the (pre-)activation values of the original NN for each class to detect potentially misclassified images. Given the set of safe activation values  $A_j^l$  for class  $j$  and layer  $l$  and the set of activation  $\bar{A}_j^l$  for images of the training data that do not lead to the class prediction, an NN, defined as  $NET_j^l$ , is created to output a score between 0 and 1 that encodes the confidence the monitoring NN has that the prediction made by the monitored NN is correct. Basing our neuron selection on the partial gradient of such a monitoring NN uses the fact that this NN has obtained a deeper understanding of the original NN.

## 5 Evaluation

In our experiments, we evaluate (RQ1) the influence of neuron selection, (RQ2) the combination of the multivariate Gaussian monitor with clustering and (RQ3) the overall performance of our suggested combination of methods.

### 5.1 Experimental Setup and Implementation

**Datasets.** For our experiments, we use two datasets, GTSRB [9], a dataset consisting of German traffic signs, and CIFAR-10 [11], which contains objects from different classes like plane, car, or bird. We evaluate our proposed monitors with the Monitizer framework [1], which allows us to implement a monitor and evaluate it on various types of OOD data. As we are interested in OMS detection, we generalize this framework by excluding OOD images from evaluation if the monitored NN still made a correct prediction and adding a new category of misclassified ID images. The OMS data classes contain images from an entirely new dataset, different noises and perturbations like light and contrast changes applied to known data, and objects not contained in the training data, but placed in a similar environment as the one known to the NN. Appendix A contains a visualization of the datasets and OMS data.

**Network Architectures.** For CIFAR-10 images, we use an NN consisting of 6 convolutional layers with ReLU activation function and max-pooling operation

followed by 4 linear layers with ReLU activation function [17]. The NN for GT-SRB consists of 2 convolutional layers with ReLU activation and max-pooling operation followed by 3 linear layers with ReLU activation function. Both architectures are illustrated in Appendix B.

**Preparation of Monitors.** For training the monitors, meaning generating the intervals and boxes, and threshold setting, we use the pre-activations of the NN for correctly classified input images, following the suggestion of previous works [3, 8]. We focus on pre-activation values as we have obtained better results on them compared to the activation values (see Appendix C). The images for threshold setting have not been used for clustering and computing intervals. We adjust our monitors’ thresholds to receive no alarm on 90% of the correctly classified ID dataset.

**Quality Measure and Plots.** The plots show the True Positive Rate (TPR) (sometimes also called *recall*) of our experiments, meaning the number of correct alarms divided by the number of OMS images for each of our OMS datasets. This is the most relevant metric as our datasets only consist of OMS examples. The monitors’ performance on data within the model-scope is fixed by the threshold.

## 5.2 Results

**RQ1: Neuron Selection.** Table 1 displays the TPR for the clustered Gaussian monitor when monitoring the pre-activation values of all neurons in the last hidden layer versus monitoring only 75%, 50% or 25% of the neurons for CIFAR-10. The results indicate that monitoring less neurons tends to decrease the TPR. However, when comparing the selection of 100% with the selection of only 25%, the decrease is mostly not significant, while reducing the number of monitored neurons by 75% drastically reduces computation efforts. Table 1 also displays the TPR when selecting 75% of the neurons for monitoring based on partial gradient descent of the monitoring NN. Our monitoring NN consists of 3 linear layers with ReLU activation function followed by one layer with Sigmoid activation function. It shows that the results obtained when using the gradients computed on the monitoring NN perform slightly better in some settings than the ones for the original NN but are mostly similar.

**RQ2: Clustering the Multivariate Gaussian [12].** Table 2 displays the TPR of the monitor when using a different number of clusters for the pre-activation values or the last hidden layer of the CIFAR-10 NN. Using clusters or increasing their number reduces performance on all test settings.

**RQ3: Overall Results.** Table 3 shows the TPR for the different monitors using the best configurations for the CIFAR-10 and the GTSRB dataset. We compare our monitors to the Gaussian monitor as Hashemi et al. [7] demonstrated that it performs at least as well as the Box monitor. Our proposed runtime monitors demonstrate better results than the Gaussian monitor in all our test settings by at least 10% on the CIFAR-10 dataset. Also on the GTSRB dataset, the clustered Gaussian monitor performs at least as well as the Gaussian monitor [7], but the

Table 1: Comparison of the TPR for the clustered Gaussian monitor with 3 Clusters when only using the  $x\%$  most relevant neurons (partial gradient descent on the original or the monitoring NN) for the pre-activation values of the last hidden layer of the CIFAR-10 NN.

Monitors	Wrong ID	GTSRB	DTD	Gaussian	SaltAndPepper	Contrast	GaussianBlur	Invert	Rotate	Light	Cifar100
Original NN											
100%	21.71	39.00	15.00	19.49	26.20	32.42	17.02	21.76	20.74	24.58	20.00
75%	17.74	44.00	13.00	13.62	12.44	28.82	9.21	14.14	13.32	22.05	17.00
50%	20.05	41.00	21.00	16.43	17.35	31.32	11.25	16.86	17.11	24.36	18.00
25%	19.59	36.00	21.00	18.34	22.89	29.58	12.05	18.73	20.27	21.99	12.00
Monitoring NN											
75%	17.67	39.00	17.00	14.75	18.51	28.42	12.62	15.81	15.07	20.77	14.00

Table 2: TPR of the multivariate Gaussian monitor applied to the pre-activation values of the last hidden layer (CIFAR-10) with different numbers of clusters.

Monitors	Wrong ID	GTSRB	DTD	Gaussian	SaltAndPepper	Contrast	GaussianBlur	Invert	Rotate	Light	Cifar100
No Clusters	24.21	57.00	12.00	18.93	15.64	42.48	12.47	21.99	20.57	34.47	25.00
2 Clusters	20.05	51.00	10.00	15.84	13.03	37.54	9.62	17.96	17.21	29.93	24.00
3 Clusters	16.20	43.00	8.00	12.90	10.63	33.48	7.34	15.03	14.29	25.19	21.00

Table 3: Comparison of the different monitors on the CIFAR-10 (top table) and the GTSRB dataset (lower table). In the first 3 rows, we consider the pre-activation values of the last hidden layer. The last row considers the activation value of the second-to-last hidden layer without clustering (similar to [7]).

Monitors	Wrong ID	GTSRB	DTD	Gaussian	SaltAndPepper	Contrast	GaussianBlur	Invert	Rotate	Light	Cifar100
Univariate Gaussian, 3 Clusters	21.71	39.00	15.00	19.49	26.20	32.42	17.02	21.76	20.74	24.58	20.00
Univariate Gaussian, No Clusters	5.20	19.00	4.00	3.37	1.56	11.99	2.53	3.99	3.18	9.13	3.00
Univariate Gaussian, [7]	10.82	19.00	4.00	7.75	5.58	19.95	4.97	8.13	6.94	15.76	8.00
Monitors	Wrong ID	CIFAR10	DTD	Gaussian	SaltAndPepper	Contrast	GaussianBlur	Rotate	Invert	Light	CTS
Univariate Gaussian, 3 Clusters	49.93	75.00	76.56	44.45	80.42	97.26	38.68	48.28	87.06	65.47	62.83
Univariate Gaussian, No Clusters	21.65	53.91	64.84	27.90	46.12	87.87	20.82	26.42	74.62	46.28	36.44
Univariate Gaussian, [7]	41.13	70.31	73.44	42.07	80.20	97.26	28.72	46.50	75.02	50.69	49.14



improvement is not as noticeable anymore. All monitors attain notably higher TPRs when assessed on the GTSRB dataset than on the CIFAR-10 dataset.

### 5.3 Discussion

Combining the research findings of Hashemi et al. [7] and Henzinger et al. [8] has demonstrated that pre-clustering the NN’s activations before constructing the Gaussian monitor is superior to a Gaussian monitor without clusters. This is particularly evident when using slightly more complex datasets, such as CIFAR-10. On the less complex GTSRB dataset the new monitor achieves at least similar results to the baseline method making our approach applicable to simpler datasets and beneficial for more complex datasets. Clustering activation values for the multivariate Gaussian monitor [12] did not improve performance.

By selecting and monitoring only the most relevant neurons, identified through partial gradient descent on several inputs, the monitor’s performance is not drastically decreased. This enables more efficient monitoring of activation values.

## 6 Conclusion and Future Work

In this work, we applied the Gaussian monitor [7] for OOD detection for NNs to the setting of OMS detection and extended it. Our new monitors consider the correlations of neurons by pre-clustering the activation values similar to [8]. We found that clustering the activation values before applying the Gaussian monitor outperforms the approach without clustering. We also saw that the number of monitored neurons can be reduced while maintaining comparable detection capabilities. This reduces the amount of computation required in each monitoring step, which is essential for executing the monitors fast. In future work, we want to evaluate on more datasets and investigate the possibility of combining monitoring of several layers.

## References

1. Azeem, M., Grobelna, M., Kanav, S., Kretinsky, J., Mohr, S., Rieder, S.: Monitizer: Automating design and evaluation of neural network monitors. arXiv preprint arXiv:2405.10350 (2024). <https://doi.org/10.48550/arXiv.2405.10350>
2. Chen, L.C., Papandreou, G., Kokkinos, I., Murphy, K., Yuille, A.L.: Deeplab: Semantic image segmentation with deep convolutional nets, atrous convolution, and fully connected crfs. *IEEE Transactions on Pattern Analysis and Machine Intelligence* **40**(4), 834–848 (2018), <https://doi.org/10.1109/TPAMI.2017.2699184>, doi: 10.1109/TPAMI.2017.2699184
3. Cheng, C.H., Nührenberg, G., Yasuoka, H.: Runtime monitoring neuron activation patterns. In: 2019 Design, Automation & Test in Europe Conference & Exhibition (DATE). pp. 300–303 (2019), <https://doi.org/10.23919/DATE.2019.8714971>, doi: 10.23919/DATE.2019.8714971
4. Cimpoi, M., Maji, S., Kokkinos, I., Mohamed, S., Vedaldi, A.: Describing textures in the wild. In: 2014 IEEE Conference on Computer Vision and Pattern Recognition. pp. 3606–3613 (2014), <https://doi.org/10.1109/CVPR.2014.461>, doi: 10.1109/CVPR.2014.461
5. Corbière, C., Thome, N., Bar-Hen, A., Cord, M., Pérez, P.: Addressing Failure Prediction by Learning Model Confidence. Curran Associates Inc., Red Hook, USA (2019), <https://dl.acm.org/doi/10.5555/3454287.3454548>, doi: 10.5555/3454287.3454548
6. Guérin, J., Delmas, K., Ferreira, R., Guiochet, J.: Out-of-distribution detection is not all you need. In: Proceedings of the Thirty-Seventh AAAI Conference on Artificial Intelligence and Thirty-Fifth Conference on Innovative Applications of Artificial Intelligence and Thirteenth Symposium on Educational Advances in Artificial Intelligence. AAAI’23/IAAI’23/EAAI’23, AAAI Press (2023), <https://doi.org/10.1609/aaai.v37i12.26732>, doi: 10.1609/aaai.v37i12.26732
7. Hashemi, V., Křetínský, J., Mohr, S., Seferis, E.: Gaussian-based runtime detection of out-of-distribution inputs for neural networks. In: Runtime Verification: 21st International Conference, RV 2021, Virtual Event, October 11–14, 2021, Proceedings. pp. 254–264. Springer, Berlin and Heidelberg, Germany (2021), [https://doi.org/10.1007/978-3-030-88494-9\\_14](https://doi.org/10.1007/978-3-030-88494-9_14), doi: 10.1007/978-3-030-88494-9\_14
8. Henzinger, T.A., Lukina, A., Schilling, C.: Outside the box: Abstraction-based monitoring of neural networks. In: De Giacomo, G., Catala, A., Dilkina, B. (eds.) ECAI 2020 : 24th European Conference on Artificial Intelligence. pp. 2433–2440. No. 325 in *Frontiers in Artificial Intelligence and Applications*, IOS Press, Amsterdam, Netherlands (2020), <https://doi.org/10.3233/FAIA200375>, doi: 10.3233/FAIA200375
9. Houben, S., Stallkamp, J., Salmen, J., Schlipsing, M., Igel, C.: Detection of traffic signs in real-world images: The German Traffic Sign Detection Benchmark. In: *International Joint Conference on Neural Networks*. No. 1288 (2013)
10. Huang, L.: Chinese traffic sign database (2023), <http://www.nlpr.ia.ac.cn/pal/trafficdata/recognition.html>, accessed on: 2023-12-20
11. Krizhevsky, A.: Learning multiple layers of features from tiny images. Tech. rep., University of Toronto, Toronto, Canada (2009)
12. Lee, K., Lee, K., Lee, H., Shin, J.: A simple unified framework for detecting out-of-distribution samples and adversarial attacks. In: *Advances in neural information processing systems*. vol. 31 (2018)

13. Liu, L., Ouyang, W., Wang, X., Fieguth, P., Chen, J., Liu, X., Pietikäinen, M.: Deep learning for generic object detection: A survey. *International Journal of Computer Vision* **128**(2), 261–318 (Feb 2020), <https://doi.org/10.1007/s11263-019-01247-4>, doi: 10.1007/s11263-019-01247-4
14. Lukina, A., Schilling, C., Henzinger, T.A.: Into the unknown: Active monitoring of neural networks. In: *International Conference on Runtime Verification*. pp. 42–61. Springer (2021)
15. Morteza, P., Li, Y.: Provable guarantees for understanding out-of-distribution detection. In: *Proceedings of the AAAI Conference on Artificial Intelligence*. vol. 36, pp. 7831–7840 (2022)
16. Ovadia, Y., Fertig, E., Ren, J., Nado, Z., Sculley, D., Nowozin, S., Dillon, J.V., Lakshminarayanan, B., Snoek, J.: Can You Trust Your Model’s Uncertainty? Evaluating Predictive Uncertainty under Dataset Shift. Curran Associates Inc., Red Hook, USA (2019), <https://dl.acm.org/doi/abs/10.5555/3454287.3455541>, doi: 10.5555/3454287.3455541
17. Ramesh, V.: Cifar-10 pytorch implementation (2021), <https://github.com/iVishalr/cifar10-pytorch>, accessed on: 2023-12-04
18. Shafaei, A., Schmidt, M.W., Little, J.: A less biased evaluation of out-of-distribution sample detectors. In: *British Machine Vision Conference* (2019), <https://doi.org/10.48550/arXiv.1809.04729>, doi: 10.48550/arXiv.1809.04729
19. Shankar, V., Dave, A., Roelofs, R., Ramanan, D., Recht, B., Schmidt, L.: Do image classifiers generalize across time? In: *2021 IEEE/CVF International Conference on Computer Vision (ICCV)*. pp. 9641–9649 (2021), <https://doi.org/10.1109/ICCV48922.2021.00952>, doi: 10.1109/ICCV48922.2021.00952
20. Sun, Y., Ming, Y., Zhu, X., Li, Y.: Out-of-distribution detection with deep nearest neighbors. In: *International Conference on Machine Learning*. pp. 20827–20840. PMLR (2022)
21. Tan, M., Le, Q.V.: Efficientnet: Rethinking model scaling for convolutional neural networks. *ArXiv* (2019), <https://doi.org/10.48550/arXiv.1905.11946>, doi: 10.48550/arXiv.1905.11946
22. Wackerly, D., Mendenhall, W., Scheaffer, R.L.: *Mathematical Statistics with Applications*. Cengage Learning (2014), isbn: 9781111798789
23. Yang, J., Zhou, K., Li, Y., Liu, Z.: Generalized out-of-distribution detection: A survey. *arXiv preprint arXiv:2110.11334* (2021)
24. Zhao, C., Sun, Q., Zhang, C., Tang, Y., Qian, F.: Monocular depth estimation based on deep learning: An overview. *Science China Technological Sciences* **63**(9), 1612–1627 (Sep 2020), <https://doi.org/10.1007/s11431-020-1582-8>, doi: 10.1007/s11431-020-1582-8

## Appendix

### A Datasets

This section gives examples of the different datasets used for our evaluation. We use two different datasets as ID data, CIFAR-10 [11] and GTSRB [9].

The CIFAR-10 dataset [11] comprises  $32 \times 32$  color images (three channels) distinguishing ten different classes. An illustration of the dataset can be found in Fig. 2.

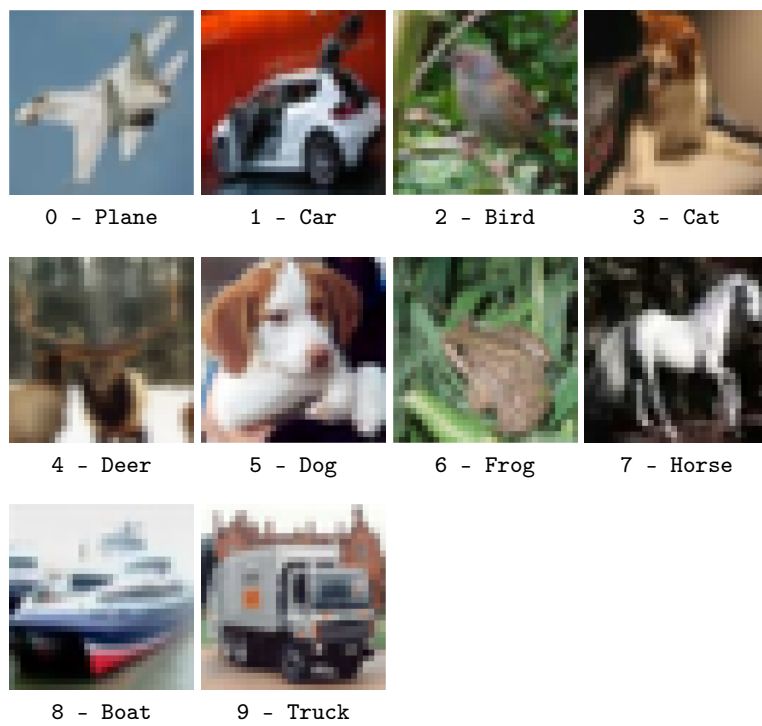


Fig. 2: Illustration of the CIFAR-10 [11] dataset.

The GTSRB [9] dataset comprises  $32 \times 32$  color images (three channels), distinguishing 43 different classes of German traffic signs. An illustration of the dataset can be found in Fig. 3.



Fig. 3: Illustration of the GTSRB [9] dataset.

Figure 4 depicts images from the ID dataset and the constructed OMS datasets for CIFAR-10. First, three datasets encode novelty: 'New World/GTSRB', 'New World/DTD', and 'Unseen Object/CIFAR100'. The DTD [4] dataset comprises images of 47 different types of textures, and CIFAR100 [11] is a disjoint dataset from CIFAR-10 consisting of 100 distinct classes. CIFAR100 is not entirely a *New World*, unlike GTSRB and DTD, as there is an overlap in the superclasses. Like CIFAR10, CIFAR100 also includes images of vehicles and animals, among other types. Secondly, seven of them encode a covariate shift: 'Gaussian Noise', 'Salt & Pepper Noise', 'Contrast Perturbation', 'Gaussian Blur Perturbation', 'Invert Perturbation', 'Rotate Perturbation' and 'Light Perturbation'.

We perform similar operations for the GTSRB dataset. Three datasets encode novelty: 'New World/GTSRB', 'New World/CTS', and 'Unseen Object/CTS'. The CTS [10] dataset includes images of various Chinese traffic signs. CTS is not entirely a 'New World', unlike CIFAR10 and

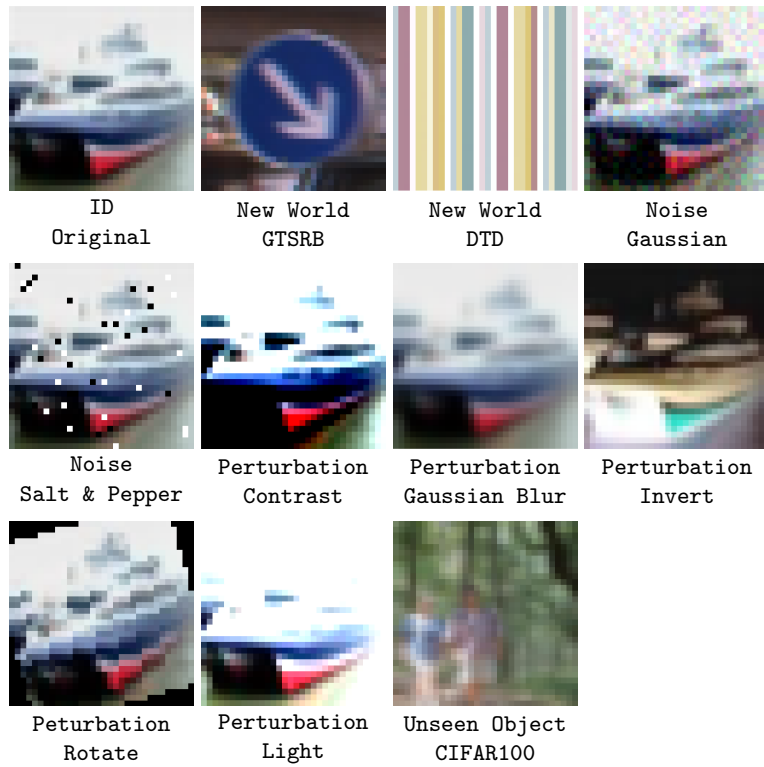


Fig. 4: Illustration of various manipulations performed on the original ID data of the CIFAR-10 dataset to create the OMS datasets.

DTD, as there is a semantical overlap. Like GTSRB, CTS also includes images of 'speed signs' or 'no parking signs' among other similar types. Secondly, seven datasets encode a covariate shift: 'Gaussian Noise', 'Salt & Pepper Noise', 'Contrast Perturbation', 'Gaussian Blur Perturbation', 'Invert Perturbation', 'Rotate Perturbation' and 'Light Perturbation'.

## B Network Architectures

This section presents the NN architectures used for evaluation in more detail. The architecture for the NN used as a classification NN for CIFAR-10 is available in Fig. 5. Figure 6 shows the architecture of the NN used for GTSRB.

Layer index $l$	Pre-Activations $Z^l$	Activations $A^l$	Number of Neurons $ L^l $
2	Conv2d()	ReLU()	-
3	Conv2d()	ReLU()	-
4	-	MaxPool2d()	-
5	Conv2d()	ReLU()	-
6	-	Dropout2d()	-
7	Conv2d()	ReLU()	-
8	-	MaxPool2d()	-
9	Conv2d()	ReLU()	-
10	-	Dropout2d()	-
11	Linear()	ReLU()	256
12	Linear()	ReLU()	128
13	Linear()	ReLU()	64
14	Linear()	-	10

Fig. 5: NN architecture for classifying images of the CIFAR-10 dataset developed by [17].

Layer index $l$	Pre-Activations $Z^l$	Activations $A^l$	Number of Neurons $ L^l $
2	Conv2d()	ReLU(BatchNorm2d())	-
4	-	MaxPool2d()	-
4	Conv2d()	ReLU(BatchNorm2d())	-
5	-	MaxPool2d()	-
6	Linear()	ReLU()	240
7	Linear()	ReLU()	84
8	Linear()	-	43

Fig. 6: NN architecture for classifying images of the GTSRB dataset, as used by Chen et al. [2] and Hashemi et al. [7].

## C Monitoring Activation and Pre-Activation Values

We evaluate whether to monitor activation or pre-activation values. We focus on hidden layers close to the output as the literature, e.g., [7, 5, 8], has found them to be the most useful ones for monitoring. Table 4 depicts the TPR of the best monitor configuration for each pre-activation and activation values  $Z^{12}$ ,  $A^{12}$ ,  $Z^{13}$  and  $A^{13}$  for the clustered Gaussian monitor on CIFAR-10. We optimized the number of clusters beforehand. The results indicate that monitoring the activation values  $Z^{12}$  and  $Z^{13}$  is more effective than monitoring the activation values  $A^{12}$  and  $A^{13}$ . Furthermore, monitoring  $Z^{13}$  instead of  $Z^{12}$  improves performance in all test scenarios for the clustered Gaussian monitor.

Table 4: Comparison of the TPR for the best configuration of the clustered Gaussian monitor trained on the pre-activation ( $Z^{12}$ ,  $Z^{13}$ ) and activation values ( $A^{12}$ ,  $A^{13}$ ) of the last two hidden layers for the CIFAR-10 NN.

Monitors	Wrong ID	GTSRB	DTD	Gaussian	SaltAndPepper	Contrast	GaussianBlur	Invert	Rotate	Light	Cifar100
$Z^{12}$ , 3 Clusters	11.78	37.00	7.00	8.75	10.69	26.77	5.18	9.57	8.27	17.51	12.00
$A^{12}$ , 2 Clusters	3.27	7.00	1.00	2.28	1.05	7.59	0.96	2.02	1.55	4.98	1.00
$Z^{13}$ , 3 Clusters	21.71	39.00	15.00	19.49	26.20	32.42	17.02	21.76	20.74	24.58	20.00
$A^{13}$ , 2 Clusters	1.58	3.00	0.00	1.28	0.44	4.04	0.33	0.92	0.64	2.45	1.00